

Exposure of a pre-damaged ITER-like Plasma Facing Unit in the WEST tokamak

Y. Corre¹, T. Loewenhoff², M. Richou¹, S. Brezinsek², J. Coenen², R. Dejarnac³, M. Diez¹, N. Fedorczak¹, M. Firdaouss¹, J. Gaspar⁴, A. Grosjean¹, C. Guillemaut¹, J. P. Gunn¹, T. Loarer¹, C. Martin⁵, G. Pintsuk², P. Reilhac¹, Q. Tichit¹, E. Tsitrone¹, M. Wirtz² and the WEST team⁶

¹ CEA, Institute for Research on Fusion by Magnetic confinement, 13108 St-Paul-Lez-Durance, France

² Forschungszentrum Jülich GmbH, Institut für Energie und Klimaforschung 52425 Jülich, Germany,

³ Institute of Plasma Physics, Czech Academy of Sciences, 182 00 Prague, Czech Republic,

⁴ Aix-Marseille Univ, CNRS, IUSTI, Marseille, France,

⁵ Aix-Marseille Université, CNRS, PIIM UMR 7345, F-13397 Marseille, France

⁶ See <http://west.cea.fr/WESTteam>

Corresponding author email address: yann.corre@cea.fr

Abstract

The consequences of tungsten (W) cracking on divertor lifetime and plasma operation are high priority issues for ITER. One actively cooled ITER-like plasma facing unit (PFU) has been pre-damaged in a High Heat Flux (HHF) facility before its installation in WEST in order to assess the damage evolution after tokamak plasma exposure. The resulting pre-damage exhibits micrometer-size crack network and high roughness on the tungsten monoblock (MB) top surface. A total of 10 MBs, equally distributed on the low and high field sides of the lower divertor, have been pre-damaged among the 35 radially aligned MBs characteristic of the WEST PFU. Subsequent plasma exposure was carried out, from the first breakdown achieved in WEST (in 2017) until the removal of the damaged PFU three years later (2020), to assess how the pre-damaged component evolves under plasma exposure and to evaluate the potential impact on plasma operation. On top of the whole WEST plasma exposure (covering C1-C4 experimental campaigns), a dedicated experiment has also been performed in the frame of the EU work program to maximize the power and energy loads on one of the damaged MBs featuring the crack network pattern. The MB top surface, including both crack network damage and “healthy” (undamaged) areas, was monitored with a high spatial resolution IR camera to detect any potential evolution of the damage pulse after pulse. This paper describes the full plasma exposure achieved in the WEST tokamak (including large number of steady-state and transient heat loading cycles), the dedicated “damaged PFU exposure” experiment together with the experimental results (heat loading on the damaged MBs). Preliminary post-mortem analysis shows that the crack network might be more pronounced after WEST steady state plasma and transients (disruption) exposures.

Keyword:

Damaged PFC, ITER like tungsten PFC, heat load, IR thermography, heat transfer modelling.

1. Introduction

Assessing how material damage can form and propagate in an ITER divertor Plasma facing Unit (PFU) under tokamak plasma exposure is an important topic to address for future ITER divertor operation. The assumption in the ITER Research Plan is that the ITER divertor lifetime should be longer than 10 years [1, 2], which corresponds

to a very large exposure time for plasma components covering the first plasma campaign (1 month), pre-fusion (39 months in hydrogen/helium plasmas) and fusion (48 months of DT plasmas) power operation. Investigating the evolution and potential degradation of ITER grade Plasma Facing Components (PFCs) in a fusion device environment is one of the key mission of the WEST tokamak [3], complementing studies performed in high heat flux facilities and linear devices [4]. In the first phase of WEST operation, few ITER-like divertor Plasma Facing Units (PFUs) have been installed and tested on the lower divertor (referred here as the test divertor sector). One of these PFUs has been pre-damaged using the JUDITH 2 HHF facility [5], using thermal shocks cycling to mimic the impact of 10^5 transients of up to 0.55 GW.m^{-2} and a duration of 0.5 ms in ITER, before its installation in WEST in 2017. Three kind of damage have been generated varying the heat flux impact factor from 3 to $12 \text{ MW/m}^2 \cdot \text{s}^{0.5}$. The damaged W grade exhibits small cracks (damage #1), crack network (damage #2) and crack network plus molten droplets (damage #3) distributed over 10 out of 35 MBs constituting one full PFU in WEST. The damage procedure and the PFU characterization performed before exposure in WEST are presented in [6]. The location of the damage on the PFU are shown in figure 1 as function of the MB number from 1 (on the high field side) to 35 (on the low field side). Subsequent plasma exposure was carried out in WEST first, with modest heat load ($< 1 \text{ MW.m}^{-2}$) to avoid compromising the C3 experimental campaign (pre-damaged PFU located in minimum heat flux area on the outer strike point). Since no significant surface aspect modification was found [6], it was decided to move the pre-damaged component to the highest heat load area for the following experimental campaign (C4). The goals of this study were to monitor the damage propagation under tokamak operation, evaluate the consequence for plasma operation with damaged PFCs, get feedback on the measurement capabilities and compare with results obtained with High Heat Flux (HHF) testing facilities. Emissivity measurement performed on the pre-damaged PFU after full tokamak exposure (C1-C4) is shown in figure 1 to illustrate the plasma footprint, including erosion and material deposition on the component [7]. On the top surface of the damage area, the mean value obtained at 50°C is 0.27 ± 0.02 . After plasma exposure, the emissivity on the pre-damage and healthy areas (here “healthy” means without pre-damage) are very close, higher than the one measured on pristine tungsten (below 0.1) [8].

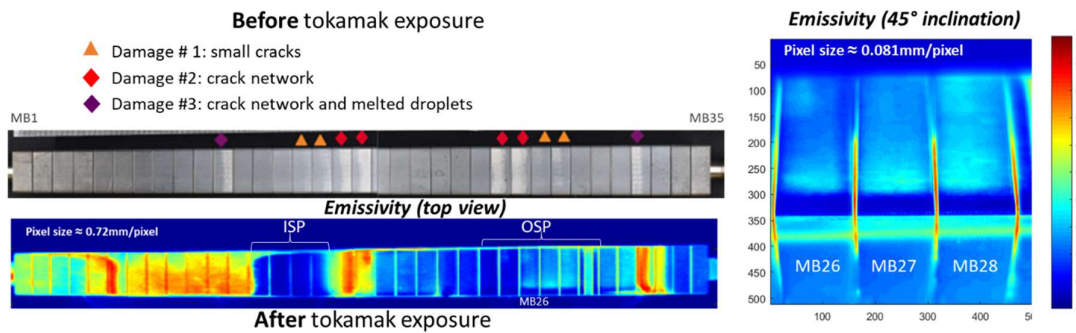


Figure 1: Pre-damaged PFU before the installation in WEST, including small cracks (MB15, 16, 27, 28), crack network (MB17, 18, 25, 26) and crack network and molten droplets (MB11 and 32) damage type. Emissivity measurement performed after tokamak exposure shows the erosion areas with lower emissivity on the inner (ISP) and outer (OSP) strike point positions. Zoom on MB26 is presented on the right picture with 45° inclination to see the exposed leading edge.

The paper is organized as follow. The experimental set-up and WEST experiments are presented in section 2. Section 3 shows the exposure of damaged PFC experiment, the heat load calculation and the very high spatial IR data. The last section shows the preliminary post-mortem analysis (confocal microscopy) after 3 years of tokamak exposure (about 6 hours of cumulated plasma duration).

2. WEST experiments overview (C1-C4 experimental campaigns)

In WEST, each PFU is made of 35 W monoblocks (see figure 1) of individual size $12\text{ mm} \times 26\text{ mm}$ (depth \times height), toroidal width varying from 28 to 32 mm on the high and low field sides, respectively, assembled with a gap of 0.5 mm on a CuCrZr heat sink tube [9]. During its first phase of operation, WEST was equipped with upper and lower divertor coils, W-coated upper divertor, baffle, inner bumper and with a flexible lower divertor made of twelve 30° sectors. One of them was equipped with actively cooled ITER-like PFUs (the test divertor sector) and the others were equipped with inertially cooled W-coated graphite PFUs to complete the divertor ring. The additional heating and current drive power is provided by high frequency heating systems, namely ion cyclotron resonance heating (ICRH) and lower hybrid current drive (LHCD), capable to deliver a nominal power up to 9 MW and 7 MW respectively. The WEST magnetic configurations allow for elongated plasmas in lower or upper single null, or double null configurations. For a standard elongated lower single null case, the X-point height ranges from 60 mm for standard operation up to 112 mm, see figure 2 (green curve), for dedicated high power operation [10]. According to the X-point height, the separatrix can reach different MBs on the inner and outer strike points as illustrated in figure 2. In the ISP area, MB 11 featuring crack network and molten droplets (damage #3) can be reached with very far X-point configuration (X point height $> 110\text{ mm}$) only, MB 15 and 16 featuring small cracks (damage #1) can be reached with standard X-point configuration while MB 17 and 18 featuring crack network (damage #2) can be reached with the close X-point configuration (X point height $< 50\text{ mm}$). In the OSP area, MB 27 and 28 featuring small cracks (damage #1) can be reached with far X-point configuration (X point height $> 90\text{ mm}$) while MB 25 and 26 featuring crack network can be reach with medium X-point height (between 70 and 90 mm).

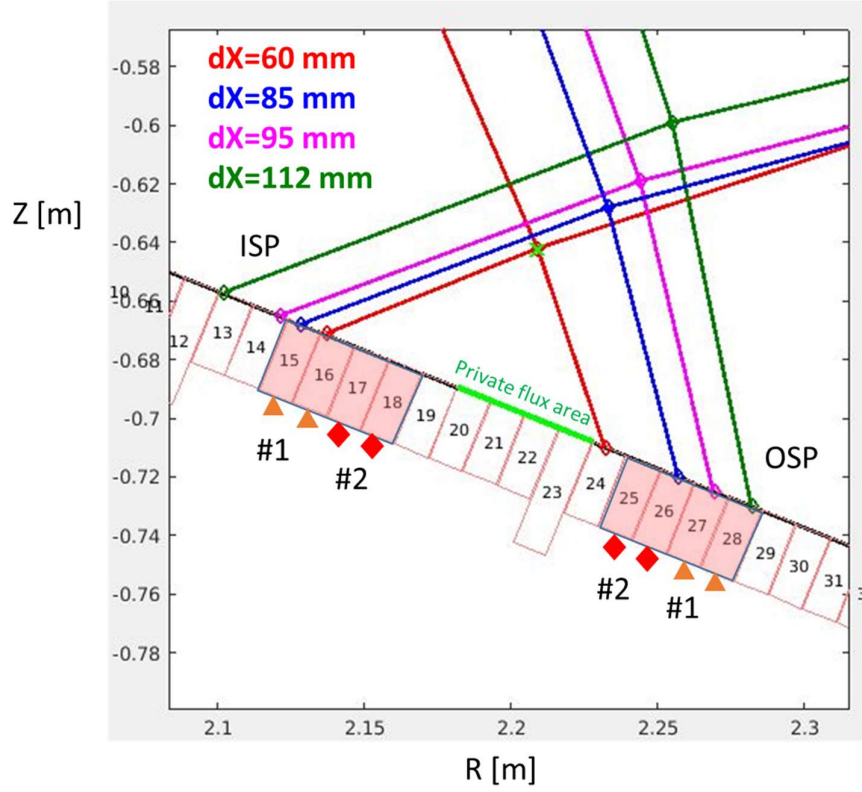


Figure 2: Lower single null magnetic configurations ($B = 3.7$ T) used in WEST: from close to far X-point (#54721 in red, #56697 in blue, #54934 in magenta, #56541 in green).

In its first operation phase with a mix of actively cooled and inertial components, WEST has performed four experimental campaigns, from C1 (2017) to C4 (2019) [11]. The first one was dedicated to the commissioning of the machine and plasma breakdown strategy (C1) [12]. The second one (C2) was dedicated to the increase of the plasma current, development of the X-point magnetic configuration and increase of the auxiliary heating systems (ICRH and LHCD). The last two experimental campaigns were dedicated to physics studies and performance improvement (C3 and C4). The main achievements performed in WEST Phase I are summarized in table 1. WEST had cumulated about 6 hours of plasma exposure and 17 GJ of injected energy. The standard scenario was a lower single null configuration, L-mode operation with divertor peak heat flux up to ~ 5 MW/m² as measured on the W-coated graphite PFUs [13]. About 2600 plasma experiments have been successfully achieved. On top of that, a large number of transients (mainly disruptions) was also reported (~ 2000 transients), each producing thermo-mechanical stresses in the PFCs. Inspection of the components after the campaign revealed a wide variety of damage at both leading and trailing monoblock edges [14] where magnetic field lines strike the MB surfaces with nearly perpendicular incidence angle. Cracking, deformation, and melting occurred.

	Nb Plasma	Ip max (kA)	Duration max (s)	Cumul (s)	Disruptions	LH total energy (MJ)	IC total energy (MJ)	Pre-damaged PFU position
C2 Nov17-Feb18	716	805	10.5	1553	282	95.5	0	PFU20
C3 July-Dec18	1076	818	37.5	7302	730	4947	105	PFU20
C4 – D2 July-Nov19	1157	1004	55	9968	755	7823	1139	PFU7
C4 - He Oct-Nov19	345	709	29	2991	275	4300	3	PFU7

Table 1: Summary of the main achievements performed in WEST phase I: number of plasma, plasma current (Ip), maximum pulse duration, cumulated plasma duration, number of disruptions, total energy injected with LHCD/ICRH systems, position of the pre-damaged PFU on the test divertor sector (see figure 3).

The monoblocks with damage #1 and #2, located in usual strike point areas, were exposed to most of the discharges of the C3 campaign while a few discharges, requiring a dedicated magnetic configuration, were performed to load the block with the most intense damage #3 on the high field side. Divertor steady state heat fluxes reached during the C3 campaign ($\sim 0.5 \text{ MW/m}^2$ on the top surface of the pre-damaged blocks, on the ISP because of the toroidal field ripple modulation as shown in figure 3) and corresponding temperatures were moderate [6]. As expected with regard to the heat loading conditions, no major surface aspect modification due to the WEST plasma exposure was found. It was therefore decided to move the pre-damaged component to the highest heat load area for the following experimental campaign (C4), taking advantage of the in/out asymmetry in divertor load. The pre-damaged PFU was therefore moved from PFU20 to PFU7 on the test divertor sector, corresponding to a maximum heat flux on the OSP.

3. High power test of ITER PFC: exposure of damaged PFC (C4)

3.1 Test divertor configuration:

For the C4 experimental campaign, the test divertor sector was equipped with 14 actively cooled ITER-like (flat top geometry) and 24 inertially cooled W coated PFUs (0.5 mm toroidal bevel geometry) as shown on figure 3-a. The damaged MBs are shown with the same symbols as used in figure 1 to distinguish the damage type (#1, #2, #3). Figure 3-b displays the heat load pattern modelled with the field line tracing code PFCflux [15] on the test divertor sector during typical plasma exposure experiment (Far X-Point configuration with $dX = 85 \text{ mm}$, 500 kA of plasma current, 4 MW auxiliary power injected in deuterium plasma #55058). The simulation was performed with heat flux decay length $\lambda_q = 10 \text{ mm}$ and outer/inner heat flux asymmetry of 4 in the divertor ($1/4$ on the inner, $3/4$ on the outer) as measured with embedded thermal measurement [13]. The plot shows the toroidal modulation of the heat flux which is observed with a 20° periodicity due to the toroidal ripple effect of the magnetic field. With the C4 divertor configuration, the MBs 24 to 28 are in the high heat flux area in the OSP, while MBs 15 to 18 are in the minimum heat flux area on the ISP.

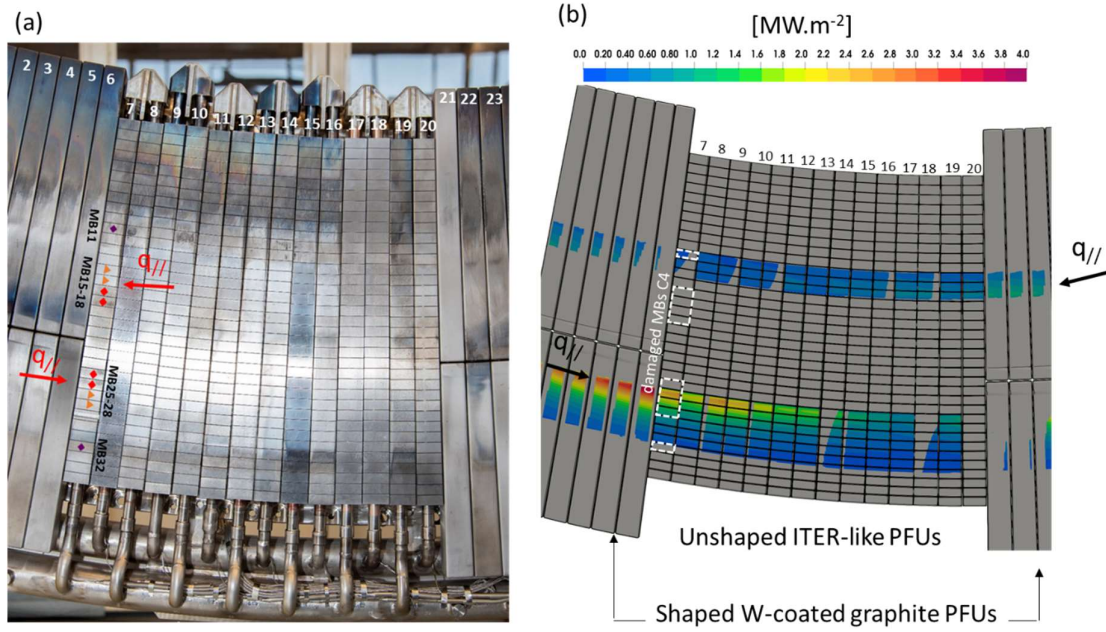


Figure 3: (a) Picture of the test divertor sector during C4 experimental campaign. (b) PFCflux simulation of the heat load with FXP magnetic equilibrium #55058 ($dX=85$ mm, $\lambda_q=10$ mm on the target, $P^{\text{SOL}}=1$ MW). Damaged PFU is located in PFU7.

3.2 C4 experimental campaign

The C4 experimental campaign is characterized by a large number of plasma (about 1500) with a significant increase of plasma power and energy compared to C3 (5 and 12 GJ cumulated injected energy in C3 and C4, respectively), plasma duration (800 and 1300 s cumulated plasma duration in C3 and C4 respectively) combined with a high disruption rate (67 %). The first part of the campaign has been performed with deuterium whilst the last two weeks have been performed with helium gas fueling. In this condition, different plasma wall interaction processes (in particular erosion and deposition pattern) have been identified and reported in [16]. Different X-point heights have been used, resulting in different inner and outer strike point locations and consequently different MB exposure (from $R=2.21$ up to 2.29 m corresponding to MB24-28 for the OSP). During C4, higher heat load on the divertor components and longer pulse duration were achieved compared to C3 [13]. Figure 4 shows the cumulated energy received by each MB during the deuterium (right) and helium (left) parts of the C4 campaign. The energy received by each MB is obtained using the WEST data base as depicted in [13]. On the OSP, MB24 (with no pre-damage) is the most loaded under deuterium plasma (standard magnetic equilibrium used in WEST). The second most loaded is the MB26 featuring crack network pre-damaging (corresponding to the magnetic equilibrium used in the dedicated exposure experiment presented in the next section). MB25 and MB27 are moderately loaded and MB28 weakly loaded with deuterium plasma. MB25 and MB26 are the most loaded under helium plasma. On the ISP, the MB16 is the most loaded. The VHR IR system was focus on the OSP (MB26), which is more loaded because of the inner and outer heat flux asymmetry ($\frac{3}{4}$ on the outer).

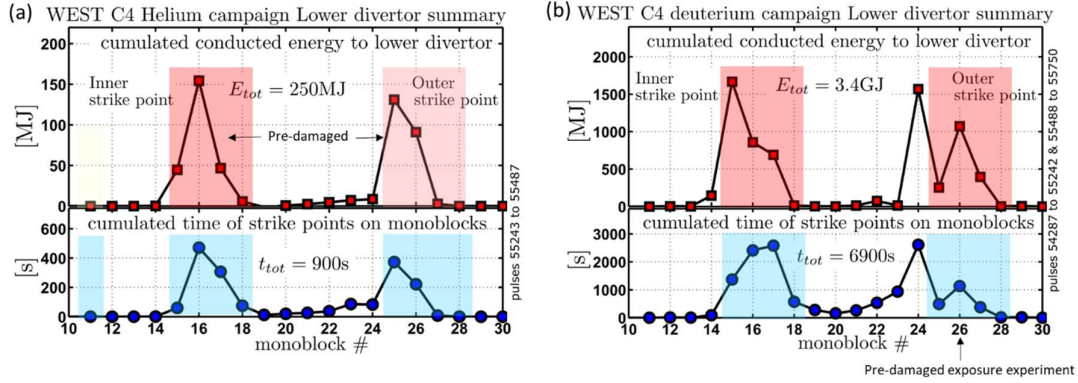


Figure 4: Accumulated energy in the C4 experimental campaign: helium (a), deuterium (b) for each MB

3.3 Repetitive exposure of the ITER pre-damage PFC

A robust steady state plasma scenario has been developed to maximize the power and energy load on one of the pre-damaged MBs featuring the crack network pattern. A series of dedicated high power steady state plasma discharges was performed in the frame of the EU work program. The X-point height was set to 85 mm from the target to put the OSP on MB26 with damage #2 (crack network). The reference pulse duration for these studies is typically 27 s, in which LHCD systems delivers 4 MW steady-state power during 20 s. Plasma parameters are: plasma current $I_p = 500$ kA, toroidal magnetic field $B = 3.6$ T, line-averaged density, $\langle n_e \rangle$, in the range of 3.8 to $4 \times 10^{19} \text{ m}^{-2}$. The radiated power fraction (f^{rad}) is in the range of 55 to 60%. Injected and radiated power are shown in figure 5 for a typical shot repeated during the experimental sessions. Each exposure shot corresponds to about 90 MJ of cumulated energy delivered to the plasma (ohmic and RF power). After the experimental session, about 600 s and 1.9 GJ of cumulated plasma exposure time and energy delivered to the plasma have been reached using the same magnetic equilibrium and plasma settings. About 30 plasma discharges have been repeated and no consequence on the plasma operation were observed. A slow and tiny increase of plasma radiation pulse to pulse has been observed, leading to a decrease of the divertor power during the sessions.

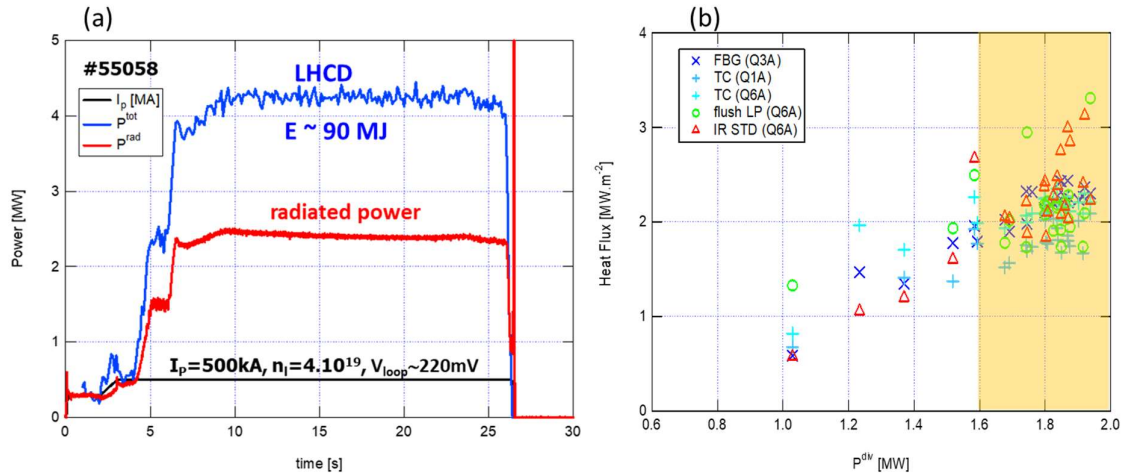


Figure 5: (a) Pulse scenario achieved for the high power exposure of ITER-like PFC: total injected power (ohmic + RF heating in blue), radiated power (in red) and plasma current in black. (b) Heat load on the top surface of the pre-damage PFU using different sensing technologies: embedded fiber Bragg grating (FBGs),

thermocouples (TC), Langmuir probe (LP) and standard IR thermography as function of the power reaching the divertor (the high power operation domain is shown in orange).

The heat loads are computed using different sensing technologies, embedded in (FBGs, TCs, LPs), or looking at the W-coated graphite PFUs (IR thermography) as depicted in [13, 17, 18]. The experimental heat loads computed on the top surface of the pre-damaged PFU are found to be in the range of $1.7 - 3.2 \text{ MW.m}^{-2}$ in the high power regime (when $P^{\text{div}} = 1.8 \pm 0.2 \text{ MW}$, orange area, figure 5-b). The heat load data scattering is quite large and could be explained by different reasons: the sensing technologies and the performances of the diagnostics are different (in particular the spatial resolution), the toroidal location of the sensors are also different in the lower divertor (even if the position regarding the toroidal magnetic ripple is the same) and the plasma properties can differ from pulse to pulse because of MHD activity, RF power coupling, impurity content and transport properties (turbulence) that could result in different electron and ion plasma temperature at the target for similar P^{div} . The pre-damaged PFU exhibits a 1 mm poloidal chamfer and a flat top surface geometry (there is no shaping as foreseen in the ITER divertor). At the OSP, the incident angle of magnetic field lines with the top surface and 1 mm chamfer are $\alpha_{\text{top}} = 2.4^\circ$ and $\alpha_{\text{ch}} = 47.4^\circ$ respectively (#55058). The heat flux on the top surface, the 1 mm chamfer and the poloidal leading edge of the block are computed with the optical approximation (OA):

$$q_n = q_{\parallel} \sin \alpha \quad (1)$$

Due to the radial misalignment of 0.3 mm of the PFU7 with regard to PFU6 (previous PFU regarding the plasma flow on the OSP), the chamfer of the leading edge is partially exposed to the plasma heat flux. Using geometrical consideration and equation (1), the heat load on top surface and exposed chamfer of MB 26 are $\sim 2.4 \text{ MW.m}^{-2}$ and $\sim 55 \text{ MW.m}^{-2}$, respectively. The temperature of the monoblock is also calculated with Finite Element Modelling (ANSYS code) using the experimental heat fluxes, both on chamfers sides and on the top surface. The heat load profile is modelled by the convolution of a Gaussian in the private flux side with an exponential function in the SOL side as depicted in [13] (S being the spreading factor and λ_q the heat flux decay length). An iterative loop is used to find the best S and λ_q that matches both the poloidal and toroidal experimental temperature profiles (see section 3.4).

3.4 Surface temperature measurement

The surface temperature measured with the Very High Resolution IR system during the dedicated exposure experiment is displayed in figure 6 assuming surface emissivity of 0.3 as extrapolated from the post-mortem analysis on the pre-damaged PFU performed at 50°C [19] to the temperature obtained during the experiment assuming an increase of emissivity of 10^{-4} per degree [8]. On the poloidal leading edge chamfer (located on the left side on the IR image), the temperature is about 800°C . On the middle of the MB, right above the cooling pipe, the temperature is found to be quite homogenous, typically between 380°C and 400°C . The cracks generated by the electron beam in the HHF test facility are of the order of few tens of micrometers size. Because of the finite pixel size (0.095 mm/pixel in the object plane) and the optical blurring and deformation [20], such cracks are too small and not visible with the VHR IR system. The picture taken after the C4 plasma exposure exhibits a complex pattern: poloidal striped lines on the left side, quite homogeneous aspect in the middle part of the MB and remaining damage marks on the right side of the MB. Toroidal cracks also appears near the 1 mm chamfer of the pre-damaged PFU and also near the sharp leading edge on the next PFU (#8) as already reported in [14, 21].

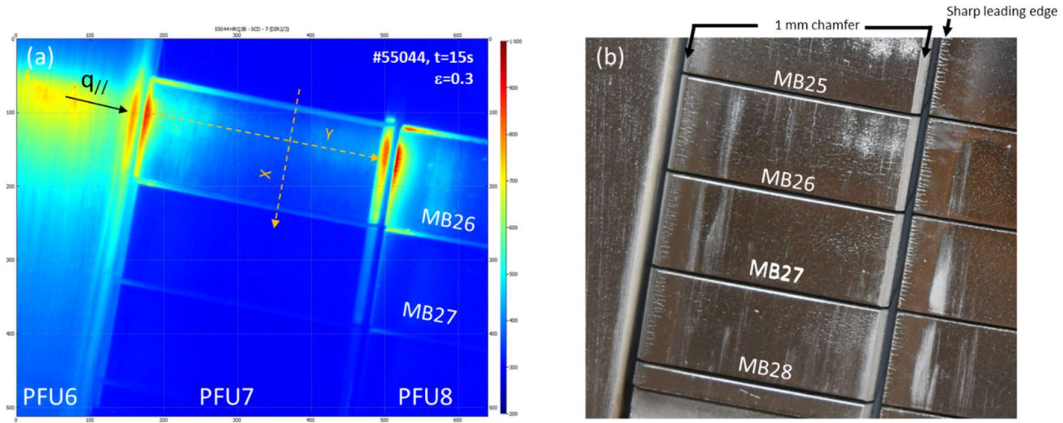


Figure 6 : (a) Surface temperature measured by the VHR IR system at $t=15s$, when the thermal equilibrium of the PFU is reached. (b) Picture of the –pre-damaged PFU taken after the C4 experimental campaign (2019).

The temperature profiles extracted from the IR image along the poloidal and toroidal directions are displayed in figure 7 for two similar pulses, one of the first (red) and one of the last (blue) pulse of the dedicated exposure sessions. On the poloidal profile (a), we observe temperature decays in both, private (left) and SOL (right) areas, suggesting a quite peaked heat load profile compared to the MB width (12 mm). The temperature found in the toroidal gaps (0.5 mm width) exhibits higher values due to the cavity effect (local increase of the emissivity in the gap because of the multi-reflexion on the two MB sides facing each other). Consequently, the absolute temperature values obtained in the gaps have no physical basis. However, such local increase of temperature is useful to localize the contour of the MB surface. The peak temperature is localized at $x = 3$ mm from the toroidal gap for the two pulses, fully on the pre-damaged area (since only half of the MB was pre-damaged). The simulation gives $S = 3$ mm and $\lambda_q = 7.5$ mm on the target to reproduce the measurement as closely as possible (black line). The heat flux decay length derived from the VHR IR system being small compared to the one derived from standard diagnostics, the peak heat load is consequently higher (5 MW.m⁻² peak heat load is required to reach 370°C on the top surface of the MB with 7.5 mm heat flux decay at the target) to keep the power received by the MB constant. The heat flux decay length is also small compared to the MB width, consequently, the healthy part located on the low field side is colder than the pre-damaged part of the MB located on the high field side and connected to the separatrix. No surface effect could be observed along the poloidal direction because of the small heat flux decay length (same heat flux would be required on both “pre-damaged” and “healthy” areas in order to make proper conclusion).

A temperature decrease of about 40°C is observed between these two pulses, which is consistent with the reduction of power in the divertor of about 10% and confirmed by the full set of embedded temperature sensors. Even if the injected power and plasma density are similar, the heat load on the divertor targets could be different because of the impurity content driving the radiated power, the residual MHD activity from the plasma start-up phase or the turbulence and heat transport properties, which could also be different from pulse to pulse. No surface evolution was therefore observed during the dedicated plasma exposure experiment.

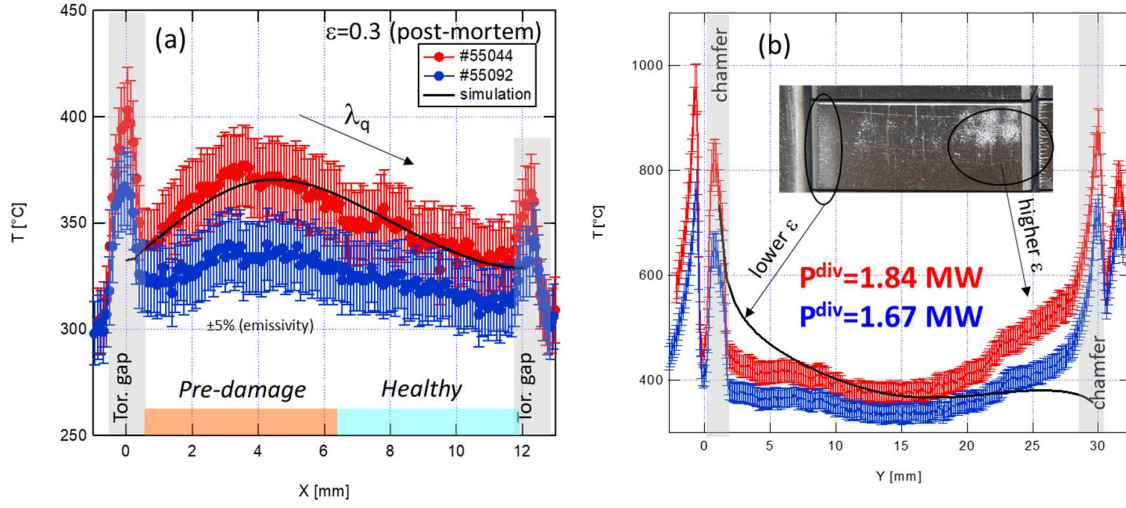


Figure 7: Poloidal (a) and toroidal (b) temperature profiles obtained during the dedicated plasma exposure experiment at the beginning (in red) and the end (in blue) of the experimental sessions, assuming constant emissivity (0.3) over the MB surface. Surface temperature obtained with ANSYS simulation is shown in black.

On the toroidal profiles (b), curved temperature profiles are observed as expected from the heat transfer modelling because of the location of the cooling pipe in the middle of the MB. The surface temperature is also higher on the trailing (right hand side) versus leading edge (left hand side), which is consistent with the surface observation and emissivity measurements (see figure 1 and [19]) performed after the plasma exposure: the pre-damaged pattern is still visible and the surface emissivity is higher ($\epsilon \sim 0.4$) on the right and smaller on the left (near the leading edge $\epsilon < 0.1$). The temperature of the chamfers are 850°C and 900°C on the leading and trailing edges, respectively, assuming the same emissivity as measured on the top surface (0.3). Such evaluation is not accurate here because of the parasitic light emitted near the pre-damaged PFU (#7) and reflected on the 1 mm chamfer, due to its inclination (45°), toward the IR camera detector located on the top of the machine as depicted in [22]. The adjacent PFUs, uncooled W-coated graphite component on the previous (#6) and misaligned sharp leading edge component on the next PFU (#8) exhibit high surface temperature, which therefore provides significant reflection near the 1 mm chamfers.

4. Post-mortem measurement: confocal microscopy

The test divertor sector that includes the pre-damage component was removed from the WEST device after the C4 experimental campaign. The actively cooled ITER like components have been removed from the test divertor sector and replaced by brand new components featuring the same shaping as foreseen in ITER (0.5 mm toroidal bevel) to prepare the transition to the fully actively cooled divertor WEST phase II. This provides the opportunity to perform post-mortem analysis on the pre-damaged areas. Preliminary results obtained with confocal microscopy in the middle of the damaged area are shown in figure 8. On the “pre-damaged” area, we observed broadening of the cracks (as pointed in yellow) and further roughening. On the “healthy” area of the top surface of the MB, we observe new and potentially deep cracks (as pointed in red) in the poloidal direction. Compared to the “healthy” area, precracking could reduce surfaces stresses that may accumulate due to a castellation of the

area in smaller sections (crack network pattern). Thermomechanical modelling and post-mortem analysis are currently ongoing in different laboratories to crosscheck the experimental results in order to make proper interpretation. Same analysis will also be performed on another and “healthy” PFU to check if the new and potentially deep cracks are also detected.

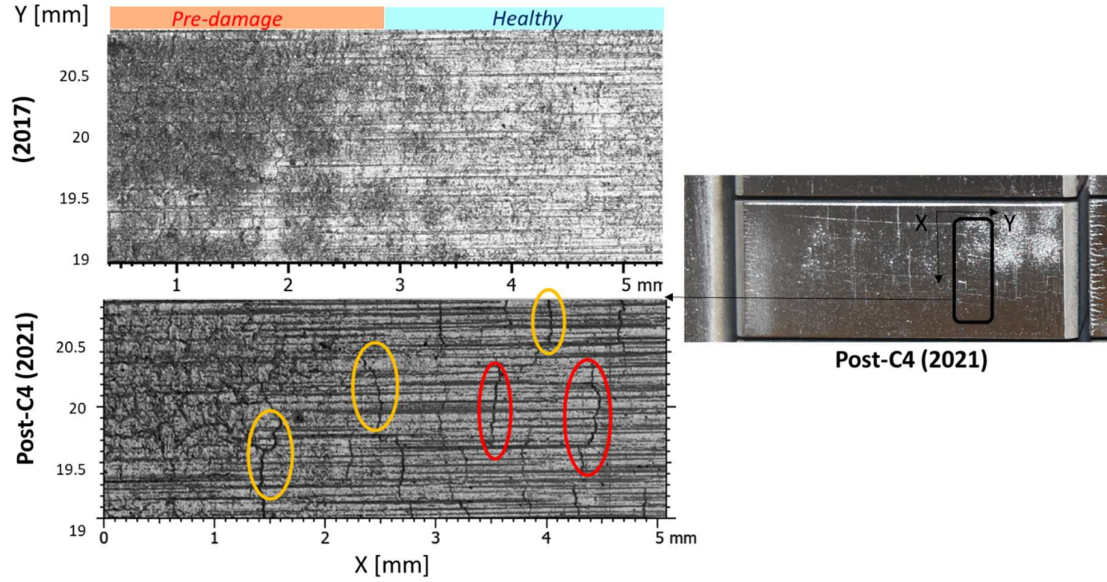


Figure 8: Confocal microscopy performed before (2017, top left) and after (2021, bottom left) tokamak exposure (spatial sampling is 645 nm). The measurement area is shown on the right (X and Y are poloidal and toroidal direction, respectively).

5. Conclusion

A robust steady state plasma scenario has been developed ($P^{\text{inj}} = 4 \text{ MW}$, $I_p = 500 \text{ kA}$, $B = 3.7 \text{ T}$) in WEST to maximize the power and energy load on the pre-damaged MBs featuring the crack network pattern. About 600 s exposure time with significant steady state heat load on the damaged area top surface have been reached using the same magnetic equilibrium and plasma setting. The heat load derived from standard and high spatial resolution (VHR IR system) diagnostics exhibit large discrepancy, 2.5 MW.m^{-2} or 5 MW.m^{-2} assuming broad or narrow heat flux decay lengths, respectively). On the micrometer scale in the crack cavity, the parallel heat flux impinging the crack could be more intense (~ 60 or 120 MW.m^{-2} assuming broad or narrow heat flux decay lengths, respectively) because of the quasi-normal incident angle of the magnetic field lines with the exposed poloidally-running leading edges (cracks featuring poloidal extension). Using the emissivity post-mortem measurement (0.3 mean value, with standard deviation ± 0.02) and VHR IR data collected during the experiment, we estimate the temperature on top surface of the damaged area to be 350°C (at the center of the MB) and higher near the 1 mm chamfer. Reduction of the power dissipated through the divertor (10%) and heat load reported on the divertor target (10% as well) are observed during the dedicated plasma exposure using the same injected power and plasma equilibrium. This is consistent with 40° temperature reduction also observed with the VHR IR system. No surface evolution has been observed or noticed during the dedicated plasma exposure. Preliminary post-mortem analysis shows broadening of the pre-damaged cracks and also new cracks on the top surface of the component after the full plasma exposure

including steady state and significant number of transient heat loads due to disruptions. Further post-mortem and thermomechanical analysis are planned to confirm this results and try to explain the mechanism involve in such evolution.

Acknowledgment

“This work has been carried out within the framework of the EUROfusion Consortium, funded by the European Union via the Euratom Research and Training Programme (Grant Agreement No 101052200 — EUROfusion). Views and opinions expressed are however those of the author(s) only and do not necessarily reflect those of the European Union or the European Commission. Neither the European Union nor the European Commission can be held responsible for them.”

- [1] R. A. Pitts et al., “Physics basis for the first ITER tungsten divertor,” *Nucl. Mater. Energy*, vol. 20, no. February, p. 100696, 2019, doi: 10.1016/j.nme.2019.100696
- [2] ITER, “ITER Research Plan within the Staged Approach (Level III – Provisional Version)” 2018
- [3] J. Bucalossi et al., “The WEST project: Testing ITER divertor high heat flux component technology in a steady state tokamak environment,” *Fusion Eng. Des.*, vol. 89, no. 7–8, 2014, doi: 10.1016/j.fusengdes.2014.01.062
- [4] C. Linsmeier et al., “Material testing facilities and programs for plasma-facing component testing,” *Nucl. Fusion*, vol. 57, no. 9, Jun. 2017, doi: 10.1088/1741-4326/aa4feb
- [5] P. Majerus, R. Duwe, T. Hirai, W. Kühnlein, J. Linke, and M. Rödig, “The new electron beam test facility JUDITH II for high heat flux experiments on plasma facing components,” *Fusion Eng. Des.*, vol. 75–79, no. SUPPL., pp. 365–369, 2005, doi: 10.1016/j.fusengdes.2005.06.058.
- [6] M. Richou et al. « First plasma exposure of a pre-damaged ITER-like plasma-facing unit in the WEST tokamak: procedure for the PFU preparation and lessons learned” 2022 *Nucl. Fusion* 62 056010
<https://iopscience.iop.org/article/10.1088/1741-4326/ac412e>
- [7] M. Balden et al., “Erosion and redeposition patterns on entire erosion marker tiles after exposure in the first operation phase of WEST”, *Physica Scripta* 96 (2021) 124020. <https://doi.org/10.1088/1402-4896/ac2182>
- [8] J. Gaspar et al., “Emissivity measurement of tungsten plasma facing components of the WEST tokamak”, *Fusion Engineering and Design* 149 (2019) 111328. <https://doi.org/10.1016/j.fusengdes.2019.111328>
- [9] M. Missirlian et al., “The WEST project: Current status of the ITER-like tungsten divertor,” *Fusion Engineering and Design*, vol. 89, no. 7, pp. 1048–1053, Oct. 2014, doi: 10.1016/j.fusengdes.2014.01.050.
- [10] Y. Corre et al. 2021 “Sustained W-melting experiments on actively cooled ITER-like plasma facing unit in WEST”. *Phys. Scr.* 96 124057
- [11] J. Bucalossi et al. “Operating a full tungsten actively cooled tokamak: overview of WEST first phase of operation”. 2022 *Nucl. Fusion* 62 042007
- [12] P. Moreau et al. “Measurements and controls implementation for WEST”. *Fusion Engineering and Design*. Volume 123, November 2017, Pages 1029-103. <https://doi.org/10.1016/j.fusengdes.2017.01.046>
- [13] J. Gaspar et al. “Divertor power loads and scrape off layer width in the large aspect ratio full tungsten tokamak WEST”. *Nucl. Fusion* 61 096027. <https://doi.org/10.1088/1741-4326/ac1803>
- [14] J. Gunn et al. “Thermal loads in gaps between ITER divertor monoblocks: First lessons learnt from WEST”.

Nuclear Materials and Energy, Volume 27, June 2021, 100920

- [15] M. Firdaouss et al. "Heat flux depositions on the WEST divertor and first wall components," Fusion Eng. Des., vol. 98–99, 2015, doi: 10.1016/j.fusengdes.2014.12.024.
- [16] E. Tsiatroni et al. "Investigation of plasma wall interactions between tungsten plasma facing components and helium plasmas in the WEST tokamak", Nuclear Fusion <https://doi.org/10.1088/1741-4326/ac2ef3>
- [17] J. Gaspar et al., "Surface heat flux estimation with embedded fiber Bragg gratings measurements: Numerical study," Nucl. Mater. Energy, vol. 12, pp. 1077–1081, 2017, doi: 10.1016/j.nme.2016.10.015
- [18] N. Fedorczak et al. "Cross diagnostics measurements of heat load profiles on the lower tungsten divertor of WEST in L-mode experiments". Nuclear Materials and Energy. Volume 27, June 2021, 100961
<https://doi.org/10.1016/j.nme.2021.100961>
- [19] J. Gaspar et al. Overview of the emissivity measurements performed in WEST: in-situ and post-mortem observations. Nuclear Fusion, accepted.
- [20] Y. Corre et al. "Methodology for heat flux investigation on leading edges using infrared thermography". Nucl. Fusion 57 (2017) 016009 (9pp)
- [21] A. Durif et al. "Leading edge cracking observed in WEST" 2022 Phys. Scr. 97 074004
- [22] A. Grosjean et al. "Interpretation of temperature distribution observed on W-ITER-like PFUs in WEST monitored with a very-high-resolution IR system". Fusion Engineering and Design 168 (2021) 112387